2022

Synergy of neuro-fuzzy controller and tuna swarm algorithm for maximizing the overall efficiency of PEM fuel cells stack including dynamic performance

Hossam Ashraf
hossam.ashraf@bue.edu.eg

Mahmoud M. Elkholy Prof
Zagazig University, melkholy71@yahoo.com

Sameh O. Abdellatif

Attia A. El-Fergany Prof
Zagazig University, el_fergany@ieee.org

Energy Conversion and Management: X 16 (2022) 100301

Contents lists available at ScienceDirect

Energy Conversion and Management: X

journal homepage: www.sciencedirect.com/journal/energy-conversion-and-management-x

Synergy of neuro-fuzzy controller and tuna swarm algorithm for maximizing the overall efficiency of PEM fuel cells stack including dynamic performance

Hossam Ashraf [a], Mahmoud M. Elkholy [b], Sameh O. Abdellatif [a], Attia A. El-Fergany [b,*]

[a] Electrical Engineering Department, Faculty of Engineering and FabLab in the Centre for Emerging Learning Technologies (CELT), The British University in Egypt (BUE), Cairo, Egypt
[b] Electrical Power and Machines Department, Zagazig University, 44519 Zagazig, Egypt

ARTICLE INFO

Keywords:
Proton exchange membrane fuel cells
Efficiency maximization
Energy saving
Dynamic model
Tuna swarm algorithm
Neuro-fuzzy

ABSTRACT

Recently, world endeavors are focused on promoting energy savings by operating both sources and loads at their maximum efficiency points. Thus, this paper presents a novel attempt to optimally determine the operating parameters of an isolated system comprising the proton exchange membrane fuel cells (PEMFCs) stack serving a variable load. A fitness function is adapted to maximize the PEMFCs stack's efficiency using tuna swarm algorithm (TSA), subjected to set of inequality constraints. A well-known commercial type of PEMFCs stack namely Nedstack PS6 6 kW, is carefully studied over two TSA-based optimization scenarios. The first scenario aims at optimizing five operating parameters, while only two operating parameters are optimized in the second one. Numerical comparisons among the two scenarios are made. It's worth indicating that the maximum absolute efficiency deviation between both scenarios is equal to 0.8064 at 100 °C. Moreover, statistical tests are executed to appraise the performance of the TSA and others. At later stage, the TSA-based results are employed to train and learn an adaptive neuro-fuzzy controller for extracting the optimal operating parameters over wider range of loading conditions, while keeping the goal of maximum efficiency point in order. This allows predicting the optimal values of the operating parameters according to a certain load with a very low time burden, making it able to simulate the real-time load variations effectively and accurately. It can be reported here at low loading values as actual results for example, at 30 % loading condition, the stack's efficiency is improved from 16.27 % to 63.47 % at 60 °C, from 17.24 % to 64.24 % at 80 °C and from 18.22 % to 65.26 % at 100 °C. While, at load power of 40 %, the FC's efficiency is enhanced from 21.65 % to 62.72 % at 60 °C, from 22.95 % to 63.60 % at 80 °C and from 24.25 % to 64.76 % at 100 °C. It may be established that via this proposed synergy between TSA and neuro-fuzzy controller, the efficiency of PEMFCs can be maximized.

1. Introduction

Recently, fossil fuels have shown ecologically destructive impacts, such as global warming, and acidic rains, due to their poisonous emissions, principally CO_2. Besides, such fuels are existed in a limited amount which threatens energy sustainability as the energy demands are rapidly increasing. Consequently, the main challenge the world faces is to replace such conventional running out sources with renewable energy sources (RESs) [1,2].

Particularly, fuel cells (FCs) are one of the RESs, which utilize hydrogen, which is the most plentiful element universally, to generate electricity by performing electrochemical reactions. FCs' systems are distinguished by higher efficiencies and energy densities, static nature, and almost no environmental issues. Moreover, FCs are convenient for portable, traction, and stationary applications either for domestic, commercial, or industrial sectors [3,4]. Additionally, the absence of the combustion and mechanical processes gives the superiority of FC

Abbreviations: RESs, Renewable energy Sources; FCs, Fuel Cells; PEMFCs, Proton Exchange Membrane Fuel Cells; EVs, Electric Vehicles; BC, Boost Converter; AI, Artificial Intelligence; GWO, Grey Wolf Optimizer; PSO, Particle Swarm Optimizer; RMSE, Root Mean Square Error; MHAs, Metaheuristic Algorithms; TSA, Tuna Swarm Algorithm; OPs, Operating Parameters; ANFIS, Adaptive Neuro-Fuzzy Inference System; CF, Cost function; ILs, Inequality Limits; AHO, Artificial Hummingbird Optimizer; ANN, Artificial Neural Network; CFAFR, Constant Fuel and Air Flow Rate.

* Corresponding author.
E-mail addresses: el_fergany@ieee.org, el_fergany@zu.edu.eg (A.A. El-Fergany).

https://doi.org/10.1016/j.ecmx.2022.100301
Received 26 May 2022; Received in revised form 15 September 2022; Accepted 16 September 2022
Available online 17 September 2022

Nomenclatures

V_s	Output voltage of PEMFC stack (V)
K_v	Voltage constant at rated conditions
E_{th}	Thermodynamic balance voltage (V)
N_c	Number of series connected cells per stack
S_t	Tafel slope (V)
i_{fc}	FC operating current (A)
i_e	Exchange current (A)
τ_d	Response time (s)
R_Ω	Overall resistance (Ω)
T_{fc}	Stack temperature (K)
P_{H_2}, and P_{O_2}	Partial pressures of H_2 and O_2 (atm), respectively
x%, and y%	Percentages of H_2 and O_2 in the fuel and air, respectively
P_f, and P_a	Absolute supply pressures of the fuel and air (atm), respectively
F_{UH_2}, and F_{UO_2}	Utilization factors of H_2 and O_2, respectively
Q_f, and Q_a	Fuel and air flow rates (l/m), respectively
F	96,485 $Asec/mol$
R	8.314 $J/(molK)$
σ	Number of moving electrons ($\sigma = 2$)
P_s	Stack output power (W)
η_{th}, η_v, and η_f	Thermodynamic, voltage and fuel efficiencies, respectively
ΔG	Change in Gibbs free energy (J)
ΔH_{HHV}	Enthalpy change at higher heating value (J)
V_{out}	Converter output voltage (V)
V_{in}	Converter input voltage (V)
D_C	Converter duty cycle
N_p	Population size
X_i	i^{th} initial agent
ul, and ll	Upper and lower limits of the search space
it	Iteration counter
it_m	Maximum number of iterations
X_b^{it}	Best agent location
β_1, and β_2	Weight factors
c	Constant
p	Probability factor
F_b	Best fitness value
$r_i (i = 1:2)$	Stochastic/random numbers from 0 to 1
r_3	Stochastic/random number from −1 to 1

efficiency, compared to heat combustion engines. Differently from batteries, FCs are not storage devices such that the electricity production is conditioned to the continuity of the fuel (hydrogen) [5].

FCs are classified into diverse types according to the electrolyte substance [3–5]. The most commercial types are (a) alkaline FCs [6], (b) molten carbonate FCs [7], (c) phosphoric acid FCs [8], (d) proton exchange membrane FCs (PEMFCs) [4], (e) solid oxide FCs [9], and many more [1]. Each is characterized by specific operation features such as operating temperature, range of output power, electrical efficiency, and suitable applications [10].

Specifically, PEMFCs surpass the other types in penetrating the commercial markets, especially in transportation applications. Their prevalence in electric vehicles (EVs) scope is own to their amazing characteristics such as: low operating temperatures, and pressures, low startup time, rapid reaction for load deviations, high-power density, compact size, and no safety concerns [1–5,11]. However, there are still further improvements in PEMFCs technology to reduce their expensive cost concentrated on the catalyst material [1]. Furthermore, the output voltage per single cell has a range of 0.8 to 1.22 V, so the voltage, and power are upgraded by serially connecting PEMFCs [12]. Over and above, this terminal voltage is unregulated and nonlinearly decays with increasing the load caused by the polarization losses (activation, ohmic, and concentration) [13]. For that reason, a DC/DC boost converter (BC) is required to step up the voltage to an appropriate value, needed by the load, and stabilize this value upon loading variations [12,14].

To properly employ FCs in EVs' systems, several factors shall be deemed, like FC performance, modularity, durability, reliability, cost, and fuel sustainability. As a result of the complexity, and the high-cost of such applications, precise modeling is mandatory before starting the design process and manufacturing prototypes [5,11]. By modeling and simulating FC systems, the analysis of the system attitudes and the assessment of the system performance under various operating conditions can be studied accurately and effectively. Additionally, varying the operation parameters for obtaining maximum efficiency and energy-saving can be determined without going through expensive experimental setups [15,16].

Accordingly, many researchers have developed mathematical models for the purpose of investigating the above-mentioned aspects of PEMFCs. Amphlett et al [17] have introduced a semi-empirical static model that simulates the polarization characteristics of PEMFCs with a good fitness between the calculated V-I datasets and the measured datasets. Nevertheless, it requires very specific input parameters, such as membrane thickness, which aren't commonly found in the manufacturer's datasheets. Moreover, the authors [18] have designed a dynamic model that is consisting of a set of resistances and capacitances in series and parallel connections. This sophisticated model gives precise results, but experimental data for real PEMFCs is needed to compute its parameters. On the other hand, a simplified dynamic model in which all the parasitic capacitors are gathered in one capacitor is represented [19]. It composes of a single capacitance parallel with two resistances to emulate the activation, and concentration losses. Furthermore, the effect of load variation on the V-I curves and the hydrogen consumption is investigated in the model proposed by [20]. For more examples of PEMFC's models, the readers are invited to visit [21–26].

As earlier-stated, such models include some undefined parameters which aren't specified in the PEMFC's datasheets. The model robustness and effectiveness depend on how accurate the estimation of these parameters is [5,11]. Consequently, many researchers have attempted to identify them by utilizing different ways such as electrochemical impedance spectroscopy methods [27,28], black box-based techniques [29,30], adaptive filter-dependent methods [31–33], and current switching-based approaches [34]. Nonetheless, they aren't commonly applied in estimating the unknown parameters of PEMFC's models, as they lack flexibility and practicability [4].

Among the various illustrated models, the one derived by Motapon et al [35] has acquired a good reputation for describing the transient response of PEMFCs and the impact of the load changing on the fuel consumption and the polarization curves. Also, this simple model has mathematically covered the thermodynamic phenomenon and the effect of charging the double layer. Thus, it has shown a significant potency in imitating the PEMFCs operating characteristics, especially those that are used in EVs' applications.

Like other models, Motapon's model suffers from the nonlinearity exhibited by the PEMFC's activation and ohmic losses, besides the model parameters' dependency on the operating conditions. Hence, determining such parameters using the aforesaid traditional methods has become more complicated and time-consuming. Therefore, the artificial intelligence (AI)-based techniques have replaced the conventional ones due to their simple construction, accurate and effective results, and low execution time [2–4,8,15,16]. Thence, a significant number of

researchers have applied Metaheuristic-based approaches (MHAs) for calculating the unknown parameters of the PEMFC models, as reported in [36–40]. When defining the parameter estimation task as an optimization problem, MHAs are the most robust and potent tool to be implemented. Referring to the no free-lunch theorem [41], all the MHAs compete to reach the global optimum solution with fast and steady convergence trends and low computational burdens without falling into local minima.

It's worth indicating that recent attempts are carried out for optimizing the PEMFC efficiency [42–46]. For example, a model predictive control technique is suggested in [47] to enhance the temperature and voltage management of PEMFC by tunning the mass flow rate of the supply fuel and cooling water. A parametric analysis, based on the engineering equation solver, is presented in [48] to study the effects of augmenting the current density on the PEMFC's overall efficiency. A multi-objective MHA is presented in [49] to improve the PEMFC's output power and efficiency and minimize the ecological effects and cost. The authors in [50] have investigated how the power density and the efficiency are affected by increasing the pores per inch of nickel metal foam. However, most of the previous-reported short survey lack assessing the influence of load changing on the PEMFC's efficiency and how to preserve maximum efficiency during such load variations.

Therefore, the authors are motivated to employ a novel swarm-based MHA, called tuna swarm algorithm (TSA), for optimizing energy-saving by maximizing overall efficiency of the PEMFCs stack. Herein, Motapon's model is chosen to properly simulate the PEMFC due to its earlier-mentioned merits. Essentially, TSA is adopted to optimally extract the values of the operating parameters (OPs) for a well-known commercial PEMFCs unit, called Nedstack PS6 6 kW, upon various loading scenarios. OPs refer to those parameters that are adjusted during the PEMFCs operation to obtain the targeted output for a certain application. It's worth stating that the TSA exhibits a smooth and fast convergence rate and effective balancing between exploration and exploitation phases.

Generally, the main contributions of the article are shortlisted as follows: i) Operating the PEMFCs stack at its maximum efficiency points regardless of the load variations via tuning set of physical parameters, ii) Deciding on the dominant parameters affecting stack efficiency to develop an adaptive and robust controller, iii) Applying a recent MHA, so-called TSA, to track the maximum efficiency points under various loading scenarios, and iv) The Adaptive Neuro-Fuzzy Inference System (ANFIS) is used to construct an adaptive controller to have maximum PEMFC efficiency regardless of loading conditions to suit of real time application.

The rest of the paper's text is arranged as follows: Section 2 illustrates the supposed system components along with their modelling formulations. The adapted cost function (CF) and the corresponding bounds are described in Section 3. Section 4 indicates the inspiration and the main steps of TSA. Section 5 presents a set of numerical simulations and results for various optimization scenarios and strategies, besides applying some statistical measures to test the TSA performance. Finally, Section 6 announces the conclusion and the sights to extend this current effort.

2. System identification and modelling

The proposed system comprises a variable resistive load supplied by PEMFCs stack via BC. At each output power level, the OPs including fuel and air flow rates, fuel and air pressures, and stack temperature, are optimized to track the maximum efficiency point of the stack. Various scenarios related to OPs are introduced by excluding some of them from the optimization process and then, measuring the corresponding maximum efficiency deviations. The overall system, whose block diagram is depicted in Fig. 1, is simulated and made ready using MATLAB/SIMULINK environment.

2.1. PEMFC's mathematical model

As earlier-reported, Motapon's [35] model is applied here to dynamically describe the PEMFC's voltage deviations while changing the load current. This model includes a constant resistance, which represent the ohmic losses, series with a controlled voltage source. Here, the PEMFC's output voltage is supposed to be affected by the activation losses due to the initial slowness of the chemical reactions, and the ohmic losses due to the electrodes and electrolyte resistivities. Accordingly, the stack voltage can be described by (1) [12].

$$V_s = K_v.E_{th} - N_c.S_t.\ln\left(\frac{i_{fc}}{i_e}\right).\left(\frac{s\tau_d}{3}+1\right)^{-1} - i_{fc}.R_\Omega \tag{1}$$

where, K_v is the voltage constant at rated conditions, N_c denotes the number of the stack series cells, S_t is the Tafel slope (V), i_{fc} is the FC operating current (A), i_e is the exchange current (A), the response time (s) and the overall resistance (Ω) are represented by τ_d and R_Ω, respectively. The open-circuit voltage due to thermodynamic balance (V) is denoted by E_{th} and given by (2) for operating temperature $\leq 100\ ^\circ$C [5].

$$E_{th} = 1.229 - 8.5\times10^{-4}\left(T_{fc}-298.15\right) + 4.3085\times10^{-5} \times T_{fc}\left[ln\left(P_{H_2}\sqrt{P_{O_2}}\right)\right] \tag{2}$$

where, T_{fc} is the stack temperature (K). The partial pressures of H_2 and O_2 (atm) are symbolized by P_{H_2} and P_{O_2}, which are determined using (3) and (4), respectively [5].

$$P_{H_2} = [1 - F_{UH_2}].x\%.P_f \tag{3}$$

$$P_{O_2} = [1 - F_{UO_2}].y\%.P_a \tag{4}$$

where, x% and y% represent the percentages of H_2 and O_2 in the fuel and air, respectively. The absolute supply pressures of the fuel and air (atm) are denoted by P_f and P_a, respectively. The utilization factors of H_2 and O_2 are indicated by F_{UH_2} and F_{UO_2}, which are calculated by (5) and

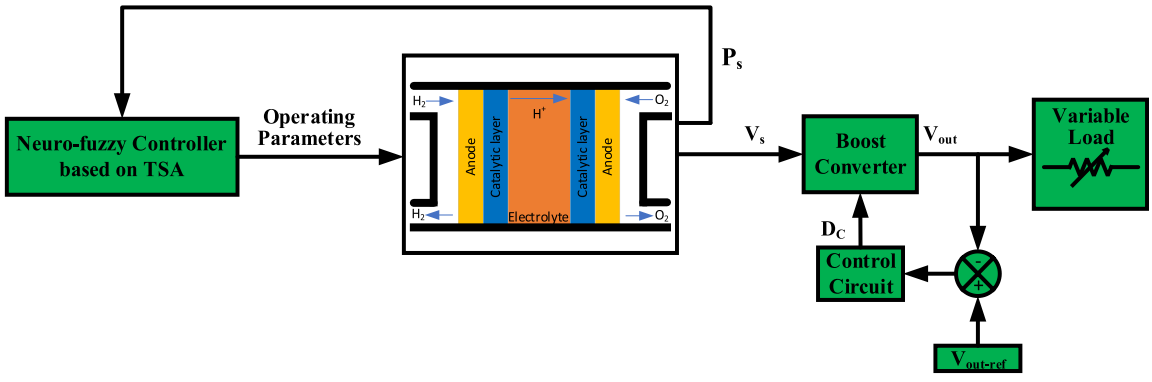

Fig. 1. Schematic diagram of the autonomous studied system.

(6), respectively [14].

$$F_{UH_2} = \frac{6 \times 10^4 . R . T_{fc} . i_{fc}}{\sigma . F . P_f . Q_f . x\%} \tag{5}$$

$$F_{UO_2} = \frac{6 \times 10^4 . R . T_{fc} . i_{fc}}{2\sigma . F . P_a . Q_a . y\%} \tag{6}$$

where, the fuel and air flow rates (l/m) are symbolized by Q_f and Q_a, respectively. F and R are equal to 96,485 $A.s/mol$ and 8.314 $J/(mol.K)$, respectively. The number of moving electrons is denoted by σ ($\sigma = 2$).

The stack output power P_s (W) can be determined by (7) [12].

$$P_s = V_s \times i_{fc} \tag{7}$$

Finally, the PEMFC overall stack efficiency η_s is described by (8) [14].

$$\eta_s = \eta_{th} \times \eta_v \times \eta_f \tag{8}$$

where, η_{th}, η_v and η_f are the thermodynamic, voltage and fuel efficiencies, which are formulated in (9), (10) and (11), respectively [14].

$$\eta_{th} = \Delta G / \Delta H_{HHV} \tag{9}$$

$$\eta_v = V_s / E_{th} \tag{10}$$

$$\eta_f = i_{fc} / (N_c . F . F_{UH_2}) \tag{11}$$

where, ΔG and ΔH_{HHV} are the change in Gibbs free energy (J) and the enthalpy change at higher heating value (J), respectively.

It's obvious that (8) doesn't consider the power consumed by the balance-of-plant devices, like compressors, that serve the PEMFC operation. Thus, the real efficiency is less than the computed one due to the power dissipated by such auxiliaries. Once again, the OPs which can be optimized for obtaining maximum η_s are Q_f, Q_a, P_f, P_a and T_{fc}.

As illustrated before, Nedstack PS6 6 kW PEMFCs stack, whose technical specifications are publicized in Table 1 (first two columns) [12], is utilized to energize an adjustable resistive load.

2.2. Boost converter model

As the nominal output voltage of the stack is 42–45 V, a DC/DC BC is employed to magnify this voltage to a suitable desired value (100 V) for supplying the load. The duty cycle (D_C) is updated using feedback control circuit, comprising a PI controller, to ensure a constant BC output voltage of 100 V, whatever the loading values. For downsizing the inductors and capacitors which results in cost reduction, the switching frequency is picked in a high value (20 kHz). It's worth mentioning that the inductor and capacitor values are equal to 0.5 mH and 7500 μ F, respectively. These settings are neatly chosen to guarantee low ripple output voltage at the stated switching frequency. The ratio of the output to the input voltages of BC is computed by (12) [12,14].

$$\frac{V_{out}}{V_{in}} = \frac{1}{1 - D_C} \tag{12}$$

Table 1
Nedstack PS6 PEMFC datasheet and the OPs' boundaries.

Stack type	Technical specifications	Practical boundaries		
	Nedstack PS6	OP	Min	Max
N_c	65	Q_f(l/m)	1	84.5
$R_\Omega(\Omega)$	0.07833	Q_a(l/m)	250	500
$i_e(A)$	0.29197	P_f(bar)	1.5	3
$x\%/y\%$	99.95/21	P_a(bar)	1	3
$\tau_d(sec)$	1	T_{fc}(K)	333	373

3. Problem identification

As earlier announced, this work targets to have optimal OPs' values of PEMFCs from energy-saving point of view under diverse loading circumstances by TSA-based method. Hence, the CF of TSA is adopted to maximize the PEMFCs stack efficiency (η_s), as given by (13).

$$CF = Minimize(100 - \eta_s) \tag{13}$$

Additionally, the proposed CF is susceptible to set of inequality limits (ILs), as depicted in (14). Also, the ILs' values, which are obtained based on the PEMFC's datasheet and presented in [12,14], are revealed in Table 1 (last three columns).

$$ILs = \begin{cases} Q_{f,min} \le Q_f \le Q_{f,max} \\ Q_{a,min} \le Q_a \le Q_{a,max} \\ P_{f,min} \le P_f \le P_{f,max} \\ P_{a,min} \le P_a \le P_a, max \\ T_{fc,min} \le T_{fc} \le T_{fc,max} \end{cases} \tag{14}$$

Needless to say, the searching space through the minimum and maximum boundaries of the afore ILs are kept by TSA (self-restrained with no extra burdens to CF).

It's worth revealing that The PEMFCs stack is the critical element in the proposed isolated system, as it's the only supply for the loads (no storage devices are included like batteries or supercapacitors). Thus, the main target of this research is to maximize the overall efficiency of the PEMFCs. Accordingly, the efficiency studied in this paper is the efficiency of the PEMFCs' stack including three sub-terms; thermal, voltage and fuel efficiencies, as depicted in equations (8) to (11). The efficiency of the DC/DC converter are not considered because the design and specification of converter can be changed according to the load requirements.

4. Overview of TSA procedures

TSA is a swarm-based MHA developed by Xie, et al in 2021. Principally, TSA mimics the intelligence behavior of tunas during their foraging process. While searching for and attacking the preys, they employ-two hunting tactics. Spiral hunting is the first tactic at which tunas force their victims to swim into shallow water for lower attacking effort by swimming in a spiral motion. The second tactic is parabolic hunting where each tuna moves after the preceding one, creating a parabolic frame to surround its victim [51].

Mathematically, like the majority of swarm-based MHAs, TSA starts by randomly and uniformly initializing the population (N_p) in the search space according to (15).

$$X_i = r_1 . (ul - ll) + ll, i \in N_p \tag{15}$$

where, X_i represents the i^{th} initial agent, ul and ll denote the upper and lower limits of the search space and r_1 is a haphazard number, uniformly generated between 0 and 1.

When the preys sense a near coming threat, they form an intensive school and continuously alter their swimming direction making it is difficult for tuna to enclose them. Thence, the tunas start to form a strict spiral shape to prosecute the preys, which is described by (16) (for $r_1 \ge it/it_m$).

$$X_i^{it+1} = \begin{cases} \beta_1 . \left(X_b^{it} + \alpha . \left|X_b^{it} - X_i^{it}\right|\right) + \beta_2 . X_i^{it}, i = 1 \\ \beta_1 . \left(X_b^{it} + \alpha . \left|X_b^{it} - X_i^{it}\right|\right) + \beta_2 . X_{i-1}^{it}, i = 2, 3, \cdots, N_p \end{cases} \tag{16}$$

$$\beta_1 = c + (1 - c) . (it/it_m) \tag{17}$$

$$\beta_2 = (1 - c) - (1 - c) . (it/it_m) \tag{18}$$

$$\alpha = e^{r_2 l} . \cos(2\pi r_2) \tag{19}$$

$$l = \exp[3\cos(((it_m + it^{-1}) - 1)\pi)] \tag{20}$$

where, it is the iteration counter, X_i^{it+1} symbolizes the position of i^{th} agent at $it+1$ iteration, the best agent location is represented by X_b^{it}, and β_1 and β_2 are weight factors that tune the agents' trend to get the positions of the best agent and the previous agent, respectively. c is a constant indicating to what extent the tunas track the best and previous agents in the initial stage. The maximum number of iterations is symbolized by it_m. r_2 is a uniform haphazard number between 0 and 1.

Particularly, the exploitation phase is achieved when all tunas perform the spiral foraging around the prey. Nevertheless, if the best agent fails to detect the prey, the group foraging won't take place as the agents impulsively follows the best agent. Consequently, a stochastic vector is generated in the search area (X_r^{it}) to direct the spiral process leading to a wider search space for each agent, which improve the exploration capability of TSA, as described by (21) (for $r_1 < it/it_m$).

$$X_i^{it+1} = \begin{cases} \beta_1.\left(X_b^{it} + \alpha.\left|X_r^{it} - X_i^{it}\right|\right) + \beta_2.X_i^{it}, i = 1 \\ \beta_1.\left(X_b^{it} + \alpha.\left|X_r^{it} - X_i^{it}\right|\right) + \beta_2.X_{i-1}^{it}, i = 2, 3, \cdots, N_p \end{cases} \quad (21)$$

Moreover, tunas also utilize the parabolic foraging in which they establish a parabolic shape with respect to the prey position. Besides, tunas can detect the victim by hunting around themselves. These two mechanisms are executed at the same time supposing that the choice likelihood is equal for both. The mathematical formulation of the two mechanisms is given by (22).

$$X_i^{it+1} = \begin{cases} X_b^{it} + r_1.\left(X_b^{it} - X_i^{it}\right) + r_3.m^2.\left(X_b^{it} - X_i^{it}\right), r_1 < 0.5 \\ r_3.m^2.X_i^{it}, r_1 \geq 0.5 \end{cases} \quad (22)$$

$$m = \left[1 - (it/it_m)\right]^{(it/it_m)} \quad (23)$$

where, r_3 is a stochastic number between -1 and 1.

Generally speaking, after the initialization process, each agent haphazardly decides whether to pick one of the two hunting tactics to implement or to reproduce its position in the search space relying on the probability (p). Furthermore, all the agents are constantly updated and determined till the stop condition is reached, then the best agent (X_b) and the corresponding fitness value (F_b) are extracted. It's worth mentioning that only $N_p, it_m, c,$ *and* p are to be fine-tuned by the user resulting in lesser computational burden and lower number of independent trials to better TSA 's performance. The overall steps of the proposed TSA are summarized in the flowchart illustrated in Fig. 2 [51].

The TSA is used to crop the optimal values of fuel cell OPs to ensure maximum efficiency of PEMFCs regardless of the range of load values. Two different scenarios are studied, the first scenario controls five parameters (Q_f, Q_a, P_f, P_a and T_{fc}). Then the second one, controls only two parameters (Q_f and Q_a) according to a certain T_{fc}. The results of TSA are employed to train and test an ANFIS to optimally predict the values of PEMFCs' OPs to attain the maximum stack efficiency for any percentage of loading.

5. Numerical simulations, and discussions

5.1. TSA-based optimization scenarios

Ten cases are studied by loading the PEMFCs unit from 10 % to 100 % of its full load power with fixed step (10 %). It's worth noticing that after many trials, the decided values of the TSA tuning parameters are $it_m = 300, N_p = 10, c = 0.7$ and $p = 0.05$. Moreover, the computer simulations are implemented via MATLAB/SIMULINK software on a laptop device with Intel Core i7 CPU, and 8 GB RAM (OS: Windows 10 Enterprise). The optimization process is subdivided into two scenarios, the first one optimizes all OPs, while the second one optimizes only two of the OPs, as illustrated in the following subsections. Finally, statistical analyses are carried out to appraise the robustness and effectiveness of TSA-based methodology.

5.1.1. Scenario (1): Five parameters

Herein, the five OPs are optimally generated, within the previous-stated boundaries, for maximizing the PEMFC's efficiency under the proposed loading values. For appraising the TSA performance, two well-matured MHAs, called grey wolf optimizer (GWO) and particle swarm optimizer (PSO) are assigned to tackle the same problem. In addition, a new MHA, called artificial hummingbird optimizer (AHO) [52], is engaged for the same previous purpose. Table 2 summarizes the TSA-based results (bolded rows) along with the AHO, GWO, and PSO-based

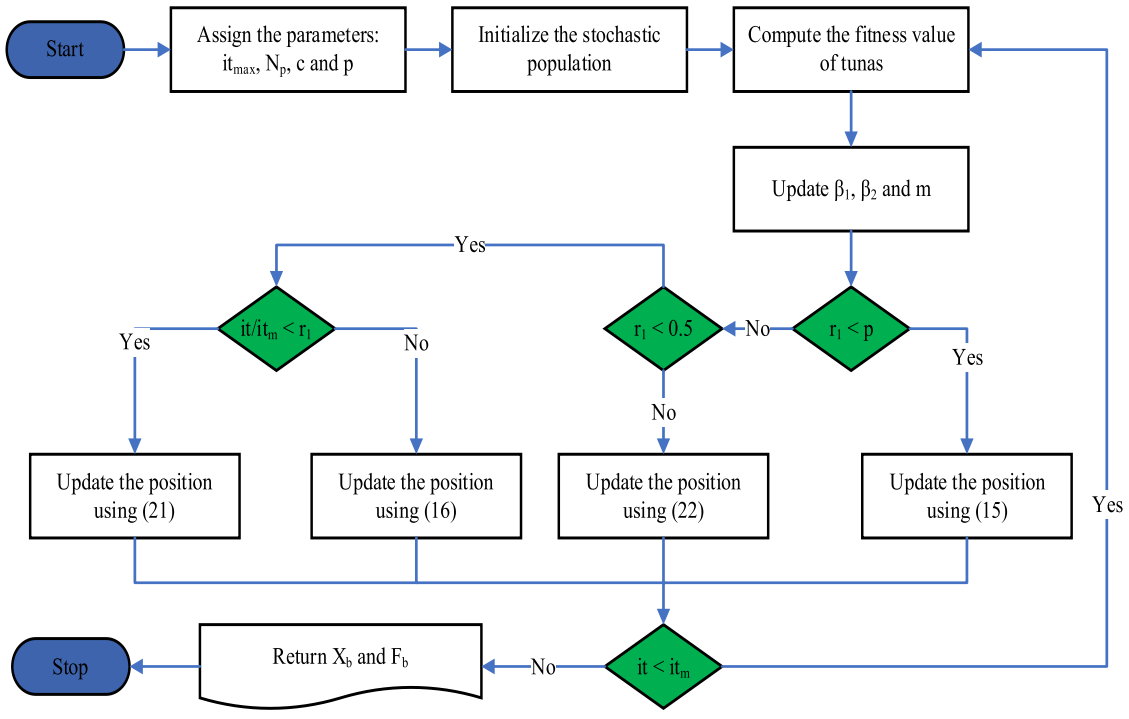

Fig. 2. The TSA's flowchart.

Table 2
TSA's results compared to AHO for scenario (1).

OPs	MHAs	Loading (%)									
		10	20	30	40	50	60	70	80	90	100
Q_f(l/m)	AHO	4.5188	8.9377	13.9632	18.6407	22.9360	28.2240	33.5807	37.5354	43.4519	48.5587
	GWO	4.6104	6.7933	13.8560	10.2967	23.5161	21.4057	20.1907	29.0192	36.0038	24.4631
	PSO	3.1460	5.4997	8.7330	18.5679	16.5125	19.9486	21.6052	30.7019	37.2738	30.8376
	TSA	**4.6084**	**9.2556**	**13.9748**	**16.8339**	**23.5582**	**28.3216**	**33.1985**	**38.1175**	**43.1079**	**24.0567**
Q_a(l/m)	AHO	438.8371	286.0088	359.3748	390.4502	353.8819	365.2811	310.4570	340.6998	488.2393	480.1582
	GWO	297.2217	373.2708	358.3679	277.6508	420.8220	500.0000	384.2643	409.9397	499.0751	314.8431
	PSO	372.0437	429.5991	347.6619	424.1461	392.5718	381.1715	370.7724	407.0021	343.6060	448.1507
	TSA	**278.7180**	**493.6435**	**252.8986**	**500.0000**	**500.0000**	**392.6029**	**401.4302**	**471.6679**	**500.0000**	**500.0000**
P_f(bar)	AHO	1.8072	2.1867	1.7041	1.8254	2.8595	1.8003	2.4867	2.6095	2.4211	2.0118
	GWO	1.5000	2.0442	1.5125	2.7216	1.5000	1.9905	2.4763	1.9728	1.8028	2.9546
	PSO	2.1419	2.3270	2.3632	1.5048	2.0739	2.0331	2.2893	1.8059	1.6860	2.3455
	TSA	**1.5610**	**2.9282**	**2.9972**	**1.6647**	**3.0000**	**2.0012**	**2.1651**	**3.0000**	**2.5913**	**3.0000**
P_a(bar)	AHO	1.5014	2.9409	2.9388	2.3983	1.8613	2.9337	1.4995	2.9961	2.2242	2.9572
	GWO	1.2335	1.0000	1.1190	2.8292	1.3786	1.1115	1.3675	2.5722	1.9611	2.9723
	PSO	2.0582	1.8954	1.9436	1.8122	2.6428	1.6782	2.4197	1.3261	1.9764	2.4966
	TSA	**2.2684**	**1.9020**	**1.0182**	**3.0000**	**1.0002**	**2.2781**	**2.9776**	**3.0000**	**3.0000**	**2.7901**
T_{fc}(K)	AHO	363.6651	358.2874	371.1818	369.7282	359.4711	369.4107	372.9919	362.7609	371.9588	372.9282
	GWO	373	373	373	373	373	373	373	373	373	373
	PSO	361.9326	337.8781	366.0341	369.2276	359.1280	348.4525	367.4539	351.1457	353.2808	373
	TSA	**373**	**373**	**373**	**373**	**373**	**373**	**373**	**373**	**373**	**373**
η_s(%)	AHO	65.8858	65.5379	65.2343	64.9638	64.1617	64.0251	63.5736	63.0390	63.0799	62.8825
	GWO	65.9182	65.6545	65.2584	65.0689	64.6179	64.1941	63.8223	63.7041	63.2106	63.0717
	PSO	65.9730	64.8559	65.1646	64.9183	64.2988	63.3073	63.8748	62.2183	62.1424	63.3403
	TSA	**66.2767**	**65.9989**	**65.5587**	**65.3932**	**64.8242**	**64.7060**	**64.3953**	**63.9199**	**63.7053**	**63.4480**

ones. Fig. 3(a)-(d) elucidate the convergence trends for four certain test cases via the implemented optimizers. It can be noted that The TSA has better CF (efficiency) than the other competitors overall 300 iterations.

For more simplicity besides minimizing the PEMFCs' auxiliaries, the succeeding subsection explains the impact of optimizing only Q_f and Q_a on the stack efficiency at certain constant T_{fc}.

5.1.2. Scenario (2): Two parameters

In this scenario, only Q_f and Q_a are optimized for attaining maximum η_s under various T_{fc} values, considering the same limits depicted in Table 1. On the other side, P_f and P_a are kept at their nominal values ($P_f = 1.5bar$ and $P_a = 1bar$). The reader can browse Table 3 to investigate the optimal values of Q_f and Q_a along with the corresponding optimized η_s for each T_{fc} value.

A closer look in Table 3, it can be recognized that η_s values are slightly lower than those of Table 2 under same conditions, for almost all loading values. For example, at $T_{fc} = 373K$, the reader can peruse the absolute deviations between the 5 optimized OPs-based η_s and the 2 OPs-based η_s along with the loading percentages, as announced in Table 4. The results indicate that the maximum deviation between the 5 optimized OPs-based efficiencies and those of 2 optimized OPs-based is 0.8064, which is an insignificant value.

5.1.3. Statistical analyses

At this moment, some statistical metrices are employed to assure the robustness, and viability of the applied TSA versus AHO, GWO, and PSO, as summarized in Table 5. It's worth stating that all these statistical indices (min, max, mean, StD, median and variance) are determined after executing all optimizers 20 independent runs. Also, to avoid paper lengthy, as representative cases, only 40 % and 100 % loadings in scenario (1) are revealed in Table 5.

Again, it's worth declaring that the ultimate target of this research is to operate the PEMFCs stack at its maximum efficiency points regardless of the load variations via tuning set of physical parameters. Accordingly, it's clear from the results that TSA has superior statistical performance rather than AHO, GWO, and PSO in terms of max, mean, and elapsed time values. On the other side, GWO has better values of min, StD, and variance.

According to Table 5 (last column), the single-run computational time for all algorithms is extremely high. This is unlogic and unapplicable for online applications where the controller shall have a very fast response to the practical load variations. Besides, such very heavy time burden represents the main reason for implementing only ten loading values (10 % to 100 % with 10 % step). However, to construct a robust and effective autonomous system, the controller shall have the ability to operate the PEMFCs' stack tracking the maximum efficiency point at any loading value (not restricted only to the ten test cases).

As a result, the authors have biased to construct an ANFIS-based controller as an adaptive controller to optimally predict the fuel and air flowrates targeting maximum stack efficiency irrespective to the load power. Specifically, the neuro-fuzzy controller is firstly trained by the data extracted from the TSA-based outcomes in scenario (2). The dependency of this controller on the TSA outcomes stems from the superiority of TSA in maximizing the stack efficiency rather than the other competitors. The extracted data is classified as input data (loading (%) and T_{fc}) and output data (Q_f and Q_a). Secondly, the controller is tested to ensure that the output data is properly linked to the input one. Now, the controller is ready to foresee the Q_f and Q_a values at any load power with a very low time burden attaining the stack maximum efficiency. The following subsection thoroughly illustrates the construction of the proposed controller, besides the obtained results.

5.2. ANFIS-based optimization approach

Basically, ANFIS is a hybrid system that integrates both artificial neural networks (ANN) and fuzzy inference systems (FIS) [53]. ANFIS popularity stems from its MATLAB-based simulation using Fuzzy Logic Toolbox with a premium graphical user interface. By applying ANFIS approach, the parameters of the membership functions and model rules can be customized according to the types and features of the system data. Also, implementing ANFIS strategy to link input data to output ones, optimally simplifies the updating process of the membership functions' parameters due to input variations. For more details about ANFIS, the reader is invited to browse [53–55].

Here, the concept of ANFIS is employed to extract the optimal values of the PEMFC fuel and air flow rates while attaining maximum PEMFC efficiency under different loading conditions and operating temperatures. The training datasets of the neuro-fuzzy controller are extracted

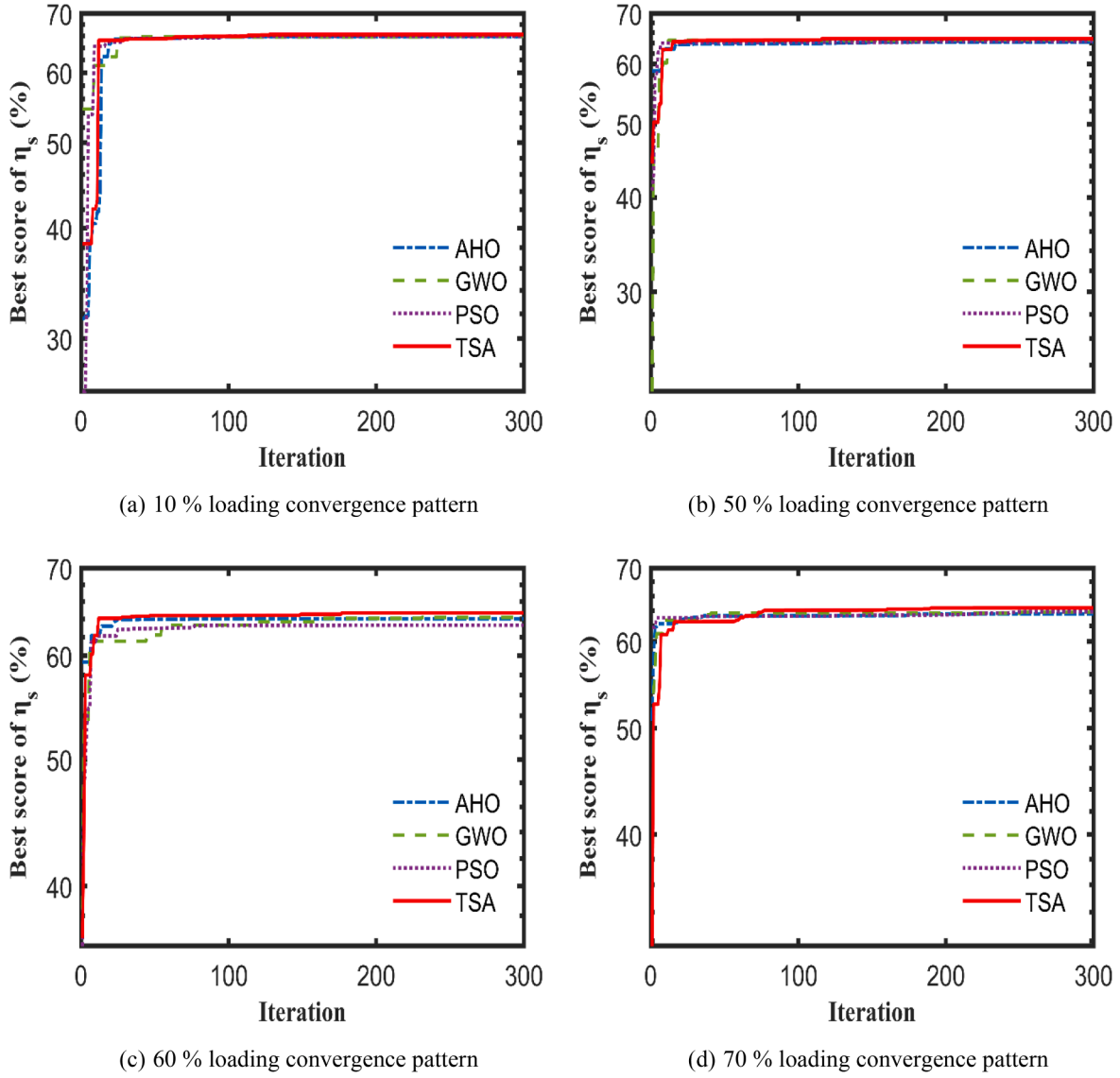

(a) 10 % loading convergence pattern

(b) 50 % loading convergence pattern

(c) 60 % loading convergence pattern

(d) 70 % loading convergence pattern

Fig. 3. Convergences trend for certain study cases.

Table 3
TSA's results for scenario (2).

$T_{fc}(K)$	OPs	Loading (%)									
		10	20	30	40	50	60	70	80	90	100
333	Q_f(l/m)	4.2025	8.4862	12.8450	17.2808	21.8216	26.4193	31.2844	36.4332	41.7570	47.5934
	Q_a(l/m)	250.000	250.292	250.021	263.540	250.000	359.450	325.923	500.000	500.000	500.000
	η_s(%)	64.8836	64.2559	63.5521	63.1166	62.4786	61.9267	61.0124	59.5763	58.7692	56.9908
343	Q_f(l/m)	4.3045	8.6839	13.1300	17.6663	22.2808	26.9150	31.7430	36.7159	41.9376	47.7895
	Q_a(l/m)	326.129	499.353	496.446	260.632	250.011	500.000	363.387	355.570	500.000	400.523
	η_s(%)	65.2442	64.6862	64.1734	63.5745	63.0284	62.6103	61.9367	61.1974	59.9751	58.7710
353	Q_f(l/m)	4.4068	8.8931	13.4405	18.0604	22.7644	27.4787	32.3225	37.2753	42.3825	47.7125
	Q_a(l/m)	500.000	250.000	322.053	316.691	265.128	500.000	500.000	481.291	460.180	477.412
	η_s(%)	65.5920	65.0064	64.5184	64.0191	63.4871	63.1150	62.5911	62.0089	61.3800	60.2968
363	Q_f(l/m)	4.5123	9.0982	13.7432	18.4627	23.2335	28.0853	33.0023	38.0450	43.1300	48.4536
	Q_a(l/m)	363.222	250.000	446.974	349.237	474.722	478.411	484.256	402.187	499.822	432.420
	η_s(%)	65.8732	65.3410	64.8850	64.3968	63.9143	63.5014	63.0224	62.5017	62.0243	61.3457
373	Q_f(l/m)	4.6092	9.2611	13.9743	18.7483	23.5869	28.4491	33.4094	38.4467	43.5524	48.7582
	Q_a(l/m)	289.962	376.866	266.565	329.312	345.668	499.993	500.000	471.280	499.995	500.000
	η_s(%)	66.2630	65.9595	65.5699	65.1645	64.7458	64.4160	63.9943	63.3162	63.0859	62.6416

Table 4
The PEMFC efficiency deviations at..$T_{fc} = 373K$

Loading %	10	20	30	40	50	60	70	80	90	100
5 OPs	66.2767	65.9989	65.5587	65.3932	64.8242	64.7060	64.3953	63.9199	63.7053	63.4480
2 OPs	66.2630	65.9595	65.5699	65.1645	64.7458	64.4160	63.9943	63.3162	63.0859	62.6416
Absolute deviations	0.0137	0.0394	0.0112	0.2287	0.0784	0.2900	0.4010	0.6037	0.6194	0.8064

Table 5
Statistical comparison between TSA and the others.

Loading %	MHAs	Statistical indices						
		Min	Max	Mean	StD	Median	Variance	Elapsed time (s)
40 %	AHO	64.2375	64.9638	64.7409	0.1911	64.7700	0.0365	1648.02
	GWO	64.9561	65.0689	65.0144	0.0350	65.0180	0.0012	2378.64
	PSO	63.7471	64.9183	64.4669	0.3187	64.5600	0.1016	2136.24
	TSA	63.9417	65.3932	65.0353	0.3609	65.1200	0.1303	1619.59
100 %	AHO	61.9853	62.8825	62.5314	0.1931	62.5310	0.0373	1339.78
	GWO	62.4877	63.0717	62.8462	0.1485	62.8670	0.0220	2448.95
	PSO	60.9667	63.3403	62.0620	0.6237	62.1420	0.3889	2283.31
	TSA	62.1616	63.4480	62.8878	0.3693	62.9700	0.1364	1282.28

from scenario (2) (See Table 3). Particularly, the input data to the controllers are the loading power and the operating temperature, while the output ones are the fuel and air flow rates. An ANFIS is constructed for each flow rate. The two controllers have the same characteristics in terms of a hidden layer with 11 neurons, as shown in Fig. 4. The triangular membership functions are utilized for the input data and the linear ones are applied for the output data. A hybrid optimization technique is picked to minimize the error goal between the desired data and the outputs of ANFIS. The convergence between the training data and ANFIS output for air and fuel flow rates is illustrated in Fig. 5(a)-(b). It may be noted that the two datasets are very close together. It's worth announcing that the root mean square error (RMSE) between the training data and ANFIS output is 0.04228 lpm for fuel flow rate and 0.37867 lpm for air flow rate.

To examine the effectiveness and accurateness of the proposed ANFIS-based system, the FC's performance, at different loading conditions, is compared with the constant fuel and air flow rates (CFAFR) method where the fuel and air flow rates are kept constant at their nominal values of 50.06 (l/m) and 300 (l/m), respectively. Three operating scenarios are elucidated at different temperatures of 60 °C, 80 °C, and 100 °C, as depicted in Fig. 6(a)-(d). The loading resistance is varied with time to change PEMFCs stack output power, as shown in Fig. 6(a). It may be noticed from Fig. 6(b) that the FC's efficiency with the proposed ANFIS controller is higher than the corresponding one of the CFAFR method. At load power of 1801 W (30 %), the FC's efficiency is improved from 16.27 % to 63.47 % at 60 °C, from 17.24 % to 64.24 % at 80 °C and from 18.22 % to 65.26 % at 100 °C. But, at load power of 2396 W (40 %), the FC's efficiency is enhanced from 21.65 % to 62.72 % at 60 °C, from 22.95 % to 63.60 % at 80 °C and from 24.25 % to 64.76 % at 100 °C. The flow rates of fuel and air are controlled according to load power, as shown in Fig. 6(c)-(d), respectively.

6. Conclusions

A novel trial to optimize the performance of an autonomous system comprising PEMFC supplying a tunable load has been presented. The dominant parameters affecting stack efficiency to develop an adaptive and robust controller have been exhibited. Predominantly, TSA has been employed to optimally extract the operating parameters of well-known PEMFCs stack, namely, Nedstack PS6, considering maximum efficiency points during various loading percentages. Additionally, Two TSA-based scenarios have been analyzed to decide the most effective operating parameters on the PEMFCs stack efficiency. Furthermore, set of statistical measurements have been carried out to signify the robustness and accurateness of the proposed TSA. Moreover, to overcome the computational time issue, a neuro-fuzzy controller has been

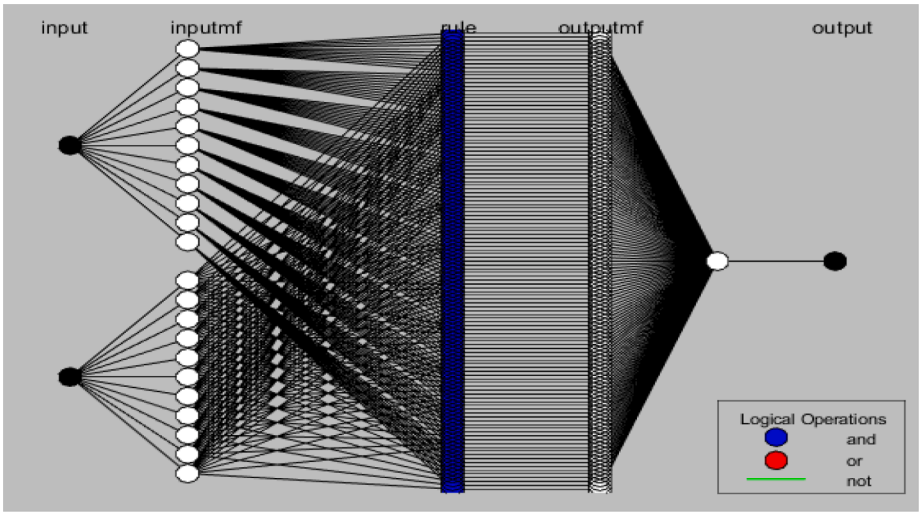

Fig. 4. The neuro-fuzzy controller structure.

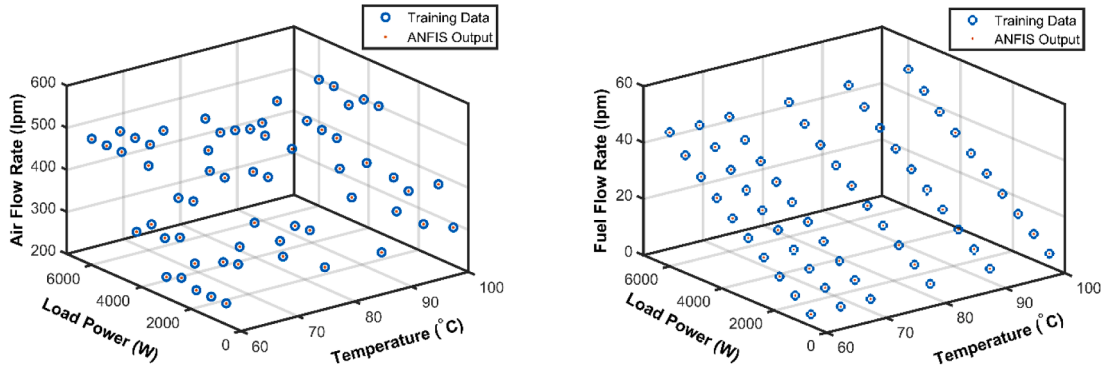

(a) Air flow rate **(b)** Fuel flow rate

Fig. 5. Variation of training data and ANFIS output.

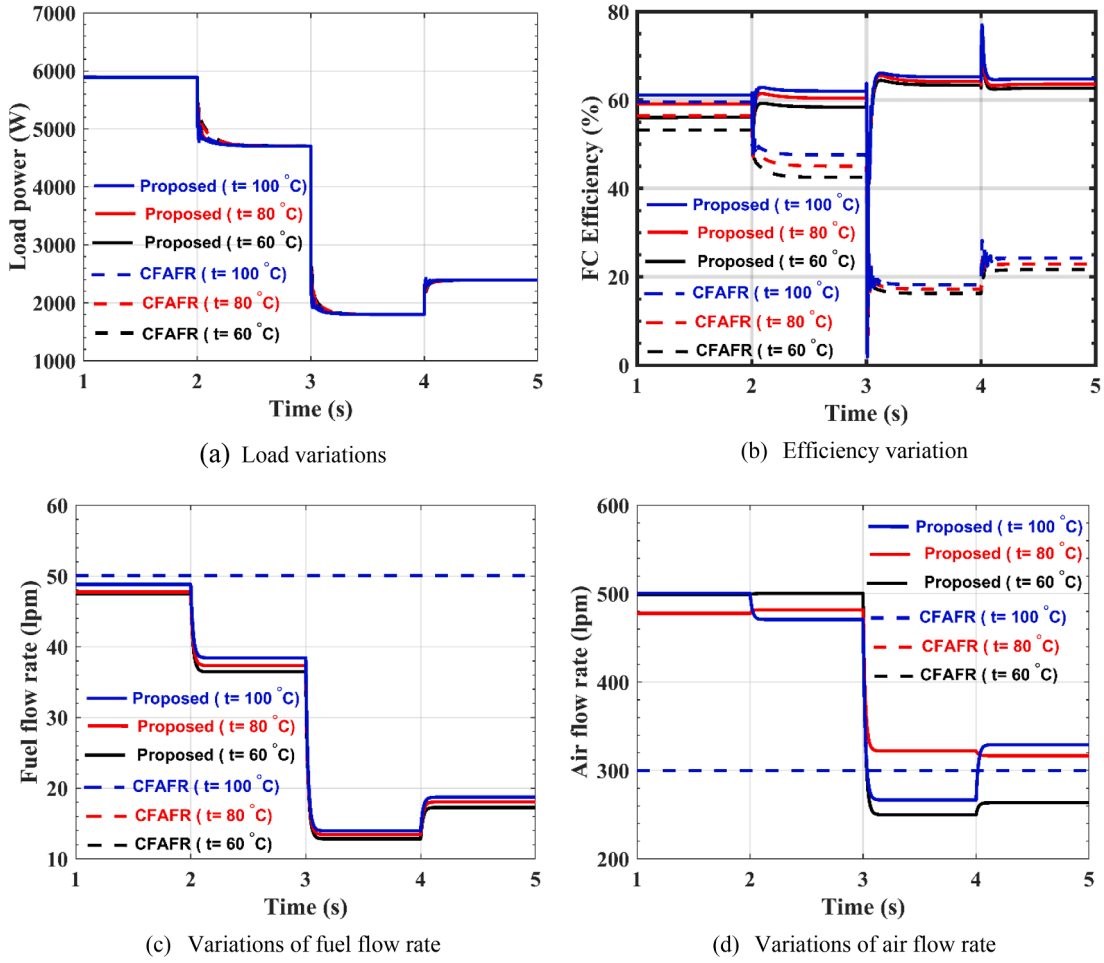

(a) Load variations (b) Efficiency variation

(c) Variations of fuel flow rate (d) Variations of air flow rate

Fig. 6. FC performance with proposed and conventional methods at different temperatures.

designed to optimally generate the fuel and air flow rates, maintaining maximum PEMFC's efficiency at different loading conditions. At 30 % loading condition, the stack's efficiency is improved from 16.27 % to 63.47 % at 60 °C, from 17.24 % to 64.24 % at 80 °C and from 18.22 % to 65.26 % at 100 °C. While, at load power of 40 %, the FC's efficiency is enhanced from 21.65 % to 62.72 % at 60 °C, from 22.95 % to 63.60 % at 80 °C and from 24.25 % to 64.76 % at 100 °C. Our future insight is to test the effectiveness of the TSA in evaluating the dynamic performance of PEMFCs stack serving an AC motor, besides assessing the impact of various motor speed control methods on the overall system efficiency.

CRediT authorship contribution statement

Hossam Ashraf: Conceptualization, Methodology, Investigation, Software, Writing – original draft. **Mahmoud M. Elkholy:** Data curation, Visualization, Software, Investigation, Validation, Writing – review & editing, Formal analysis. **Sameh O. Abdellatif:** Data curation, Validation, Software, Writing – original draft. **Attia A. El-Fergany:**

Software, Methodology, Writing – review & editing, Supervision, Validation.

Declaration of Competing Interest

The authors declare that they have no known competing financial interests or personal relationships that could have appeared to influence the work reported in this paper.

Data availability

No data was used for the research described in the article.

References

[1] Hossam Ashraf, Sameh O. Abdellatif, Mahmoud M. Elkholy, Attia A. El-Fergany. Computational techniques based on artificial intelligence for extracting optimal parameters of PEMFCs: survey and insights. Arch Computat Methods Eng (2022) In Press. https://doi.org/10.1007/s11831-022-09721-y.

[2] Karanfil G. Importance and applications of DOE/optimization methods in PEM fuel cells: a review. Int J Energy Res 2020;44:4–25. https://doi.org/10.1002/er.4815.

[3] Priya K, Sathishkumar K, Rajasekar N. A comprehensive review on parameter estimation techniques for proton exchange membrane fuel cell modelling. Renew Sustain Energy Rev 2018;93:121–44. https://doi.org/10.1016/j.rser.2018.05.017.

[4] Yang Bo, Wang J, Lei Yu, Shu H, Tao Yu, Zhang X, et al. A critical survey on proton exchange membrane fuel cell parameter estimation using meta-heuristic algorithms. J Cleaner Prod 2020;265:121660. https://doi.org/10.1016/j.jclepro.2020.121660.

[5] Abd El Monem AA, Azmy AM, Mahmoud SA. Effect of process parameters on the dynamic behavior of polymer electrolyte membrane fuel cells for electric vehicle applications. Ain Shams Eng J 2014;5(1):75–84. https://doi.org/10.1016/j.asej.2013.05.001.

[6] Saebea D, Chaiburi C, Authayanun S. Model based evaluation of alkaline anion exchange membrane fuel cells with water management. Chem Eng J 2019;374:721–9. https://doi.org/10.1016/j.cej.2019.05.200.

[7] Ido A, Kawase M. Development of a tubular molten carbonate direct carbon fuel cell and basic cell performance. J Power Sources 2020;449:227483. https://doi.org/10.1016/j.jpowsour.2019.227483.

[8] Inci M, Türksoy O. Review of fuel cells to grid interface: configurations, technical challenges and trends. J Cleaner Prod 2019;213:1353–70. https://doi.org/10.1016/j.jclepro.2018.12.281.

[9] Chuahy FDF, Kokjohn SL. Solid oxide fuel cell and advanced combustion engine combined cycle: a pathway to 70% electrical efficiency. Appl Energy 235 2019:391–408. https://doi.org/10.1016/j.apenergy.2018.10.132.

[10] Elsayed SK, Agwa AM, Elattar EE, El-Fergany AA. Steady-state modelling of PEM fuel cells using gradient-based optimizer. DYNA, DYNA-ACELERADO 2021;96:520–7. https://doi.org/10.6036/10099.

[11] Kandidayeni M, Macias A, Amamou AA, Boulon L, Kelouwani S, Chaoui H. Overview and benchmark analysis of fuel cell parameters estimation for energy management purposes. J Power Sources 2018;380:92–104. https://doi.org/10.1016/j.jpowsour.2018.01.075.

[12] El-Hay EA, El-Hameed MA, El-Fergany AA. Improved performance of PEM fuel cells stack feeding switched reluctance motor using multi-objective dragonfly optimizer. Neural Comput Appl 2019;31:6909–24. https://doi.org/10.1007/s00521-018-3524-z.

[13] Seleem SI, Hasanien HM, El-Fergany AA. Equilibrium optimizer for parameter extraction of a fuel cell dynamic model. Renew Energy 2021;169:117–28. https://doi.org/10.1016/j.renene.2020.12.131.

[14] El-Hay EA, El-Hameed MA, El-Fergany AA. Performance enhancement of autonomous system comprising proton exchange membrane fuel cells and switched reluctance motor. Energy 2018;163:699–711. https://doi.org/10.1016/j.energy.2018.08.104.

[15] Kandidayeni M, Macias A, Khalatbarisoltani A, Boulon L, Kelouwani S. Benchmark of proton exchange membrane fuel cell parameters extraction with metaheuristic optimization algorithms. Energy 2019;183:912–25. https://doi.org/10.1016/j.energy.2019.06.1520360-544.

[16] Ohenoja M, Leiviska K. Observations on the parameter estimation problem of polymer electrolyte membrane fuel cell polarization curves. Fuel Cells 2020;20:516–26. https://doi.org/10.1002/fuce.201900155.

[17] Amphlett JC, Baumert RM, Mann RF, Peppley BA, Roberge PR. Performance modeling of the Ballard Mark IV solid polymer electrolyte fuel cell. J Electrochem Soc 1995;142. https://doi.org/10.1149/1.2043866.

[18] Garnier J, Pera MC, Hissel D, Harel F, Candusso D, Glandut N, Diard JP, De Bernardinis A, Kauffmann JM, Coquery G. Dynamic PEM fuel cell modeling for automotive applications. IEEE 58th Vehicular Technology Conference—VTC2003-Fall, Orlando, FL, USA, 6–9 Oct 2003, pp 3284–3288. doi: 10.1109/vetecf.2003.1286265.

[19] Rajabzadeh M, Bathaee SMT, Golkar MA. Dynamic modeling and nonlinear control of fuel cell vehicles with different hybrid power sources. Int J Hydrogen Energy 2016;41:3185–98. https://doi.org/10.1016/j.ijhydene.2015.12.046.

[20] Atlam O, Dundar G. A practical equivalent electrical circuit model for proton exchange membrane fuel cell (PEMFC) systems. Int J Hydrogen Energy 2021;46:13230–9. https://doi.org/10.1016/j.ijhydene.2021.01.108.

[21] Zhang G, Jiao K. Three-dimensional multi-phase simulation of PEMFC at high current density utilizing Eulerian-Eulerian model and two-fluid model. Energy Convers Manage 2018;176:409–21. https://doi.org/10.1016/j.enconman.2018.09.031.

[22] Peng F, Ren L, Zhao Y, Li L. Hybrid dynamic modeling-based membrane hydration analysis for the commercial high-power integrated PEMFC systems considering water transport equivalent. Energy Convers Manage 2020;205:112385. https://doi.org/10.1016/j.enconman.2019.112385.

[23] Liu G, Qin Y, Wang J, Liu C, Yin Y, Zhao J, et al. Thermodynamic modeling and analysis of a novel PEMFC-ORC combined power system. Energy Convers Manage 2020;217:112998. https://doi.org/10.1016/j.enconman.2020.112998.

[24] Chen Xi, Liu Q, Jianghai Xu, Chen Y, Li W, Yuan Z, et al. Thermodynamic study of a hybrid PEMFC-solar energy multi-generation system combined with SOEC and dual Rankine cycle. Energy Convers Manage 2020;226:113512. https://doi.org/10.1016/j.enconman.2020.113512.

[25] Xu Y, Fan R, Chang G, Xu S, Cai T. Guofeng Chang, Sichuan Xu, TaoCai. Investigating temperature-driven water transport in cathode gas diffusion media of PEMFC with a non-isothermal, two-phase model. Energy Convers Manage 2021;248:114791. https://doi.org/10.1016/j.enconman.2021.114791.

[26] Wang Y, Li H, Feng H, Han K, He S, Gao M. Simulation study on the PEMFC oxygen starvation based on the coupling algorithm of model predictive control and PID. Energy Convers Manage 2021;249:114851. https://doi.org/10.1016/j.enconman.2021.114851.

[27] Lee J, Salihi H, Lee J, Hyunchul Ju. Impedance modeling for polymer electrolyte membrane fuel cells by combining the transient two-phase fuel cell and equivalent electric circuit models. Energy 2022;239:122294. https://doi.org/10.1016/j.energy.2021.122294.

[28] Zhao L, Dai H, Pei F, Ming P, Wei X, Zhou J. A comparative study of equivalent circuit models for electro-chemical impedance spectroscopy analysis of proton exchange membrane fuel cells. Energies 2022;15:386. https://doi.org/10.3390/en15010386.

[29] Kheirandish A, Motlagh F, Shafiabady N, Dahari M. Dynamic modelling of PEM fuel cell of power electric bicycle system. Int J Hydrogen Energy 2016;41:9585–94. https://doi.org/10.1016/j.ijhydene.2016.02.046.

[30] Hu P, Cao G-Y, Zhu X-J, Li J. Xin-Jian Zhu, Jun Li. Modeling of a proton exchange membrane fuel cell based on the hybrid particle swarm optimization with Levenberg–Marquardt neural network. Simul Model Pract Theory 2010;18(5):574–88. https://doi.org/10.1016/j.simpat.2010.01.001.

[31] Ettihir K, Boulon L, Agbossou K. Energy management strategy for a fuel cell hybrid vehicle based on maximum efficiency and maximum power identification. IET Electr Syst Transp 2016;6:261–8. https://doi.org/10.1049/iet-est.2015.0023.

[32] Ettihir K, Boulon L, Agbossou K. Optimization-based energy management strategy for a fuel cell/battery hybrid power system. Appl Energy 2016;163:142–53. https://doi.org/10.1016/j.apenergy.2015.10.176.

[33] Ettihir K, Higuita Cano M, Boulon L, Agbossou K. Design of an adaptive EMS for fuel cell vehicles. Int J Hydrogen Energy 2017;42:1481–9. https://doi.org/10.1016/j.ijhydene.2016.07.211.

[34] Chang W-Y. Estimating equivalent circuit parameters of proton exchange membrane fuel cell using the current change method. Int J Electr Power Energy Sys 2013;53:584–91. https://doi.org/10.1016/j.ijepes.2013.05.031.

[35] Souleman Njoya Motapon, Olivier Tremblay. Development of a generic fuel cell model: application to a fuel cell vehicle simulation. Int.J. Power Electron. 2012;4:505–22. https://doi.org/10.1504/IJPELEC.2012.052427.

[36] Rao Y, Shao Z, Ahangarnejad AH, Gholamalizadeh E, Sobhani B. Shark smell optimizer applied to identify the optimal parameters of the proton exchange membrane fuel cell model. Energy Convers Manage 2019:1–8. https://doi.org/10.1016/j.enconman.2018.12.057.

[37] Gouda EA, Kotb MF, El-Fergany AA. Jellyfish search algorithm for extracting unknown parameters of PEM fuel cell models: steady-state performance and analysis. Energy 2021;221:119836. https://doi.org/10.1016/j.energy.2021.119836.

[38] Shaheen MAM, Hasanien HM, El Moursi MS, El-Fergany AA. Precise modeling of PEM fuel cell using improved chaotic mayfly optimization algorithm. Int J Energy Res 2021;45:18754–69. https://doi.org/10.1002/er.6987.

[39] Abdel-Basset M, Mohamed R, El-Fergany A, Chakrabortty RK, Ryan MJ. Adaptive and efficient optimization model for optimal parameters of proton exchange membrane fuel cells: a comprehensive analysis. Energy 2021;233:121096. https://doi.org/10.1016/j.energy.2021.121096.

[40] Ashraf H, Abdellatif SO, Elkholy MM, El-Fergany AA. Honey badger optimizer for extracting the ungiven parameters of PEMFC model: Steady-state assessment. Energy Convers Manage 2021;258:115521. https://doi.org/10.1016/j.enconman.2022.115521.

[41] Wolpert DH, Macready WG. No free lunch theorems for optimization. IEEE Trans Evol Comput 1997;1:67–82. https://doi.org/10.1109/4235.585893.

[42] Chen Xi, Jianghai Xu, Fang Ye, Li W, Ding Y, Wan Z, et al. Temperature and humidity management of PEM fuel cell power system using multi-input and multi-output fuzzy method. Appl Therm Eng 2022;203:117865. https://doi.org/10.1016/j.applthermaleng.2021.117865.

[43] Tiar M, Betka A, Drid S, Abdeddaim S, Becherif M, Tabandjat A. Optimal energy control of a PV-fuel cell hybrid system. Int J Hydrogen Energy 2016;42:1456–65. https://doi.org/10.1016/j.ijhydene.2016.06.113.

[44] Chen H, Yang C, Deng K, Zhou N, Haochuang Wu. Multi-objective optimization of the hybrid wind/ solar/fuel cell distributed generation system using hammersley

sequence sampling. Int J Hydrogen Energy 2017;42:7836–46. https://doi.org/10.1016/j.ijhydene.2017.01.202.
[45] Tirnovan R, Giurgea S. Efficiency improvement of a PEMFC power source by optimization of the air management. Int J Hydrogen Energy 2012;37:7745–56. https://doi.org/10.1016/j.ijhydene.2012.02.029.
[46] Bizon N. Improving the PEMFC energy efficiency by optimizing the fueling rates based on extremum seeking algorithm. Int J Hydrogen Energy 2014;39:10641–54. https://doi.org/10.1016/j.ijhydene.2014.04.194.
[47] Chen Xi, Fang Ye, Liu Q, He L, Zhao Y, Huang T, et al. Temperature and voltage dynamic control of PEMFC Stack using MPC method. Energy Rep 2022;8:798–808. https://doi.org/10.1016/j.egyr.2021.11.271.
[48] Montazerinejad H, Fakhimi E, Ghandehariun S, Ahmadi P. Advanced exergy analysis of a PEM fuel cell with hydrogen energy storage integrated with organic rankine cycle for electricity generation. Sustain Energy Technol Assess 2022;51:101885. https://doi.org/10.1016/j.seta.2021.101885.
[49] Mei B, Barnoon P, Toghraie D, Su C-H, Nguyen HC, Khan A. Energy, exergy, environmental and economic analyzes (4E) and multi-objective optimization of a PEM fuel cell equipped with coolant channels. Renew Sustain Energy Rev 2022;157:112021. https://doi.org/10.1016/j.rser.2021.112021.
[50] Chen Xi, Yang C, Sun Y, Liu Q, Wan Z, Kong X, et al. Water management and structure optimization study of nickel metal foam as flow distributors in proton exchange membrane fuel cell. Appl Energy 2022;309:118448. https://doi.org/10.1016/j.apenergy.2021.118448.
[51] Xie L, Han T, Zhou H, Zhang Z-R, Han Bo, Tang A, et al. Tuna swarm optimization: A novel swarm-based metaheuristic algorithm for global optimization. Computat Intelligen Neuroscience 2021;2021:1–22. https://doi.org/10.1155/2021/9210050.
[52] Zhao W, Wanga L, Mirjalili S. Artificial hummingbird algorithm: A new bio-inspired optimizer with its engineering applications. Comput Methods Appl Mech Eng 2022;388:114194. https://doi.org/10.1016/j.cma.2021.114194.
[53] Kheirandish A, Akbari E, Nilashi M, Dahari M. Using ANFIS technique for PEM fuel cell electric bicycle prediction model. Int J Environ Sci Technol 2019;16:7319–26. https://doi.org/10.1007/s13762-019-02392-6.
[54] Elkholy MM, Elhameed MA. Minimization of starting energy loss of three phase induction motors based on particle swarm optimization and neuro Fuzzy network. Int J Power Electron Drive Sys (IJPEDS) 2016;7:1038–48. https://ijpeds.iaescore.com/index.php/IJPEDS/article/view/5821.
[55] Sreedharan D, Paul V, Thottungal R. Mathematical modelling of polymer electrolyte membrane fuel cell and fuzzy-based intelligent controllers for performance enhancement. Comput Electr Eng 2019;77:354–65. https://doi.org/10.1016/j.compeleceng.2019.06.017.